ACS APPLIED NANO MATERIALS

www.acsanm.org Letter

Soliton Disentangling and Ferroelectric Hysteresis in Bilayer MoS_2 Nanostructures with Reconstructed Moiré Superlattices

Yanshuang Li,[▽] Huan Zeng,[▽] Xiuhua Xie,* Binghui Li, Jishan Liu, Shuangpeng Wang, Dengyang Guo, Yuanzheng Li, Weizhen Liu, and Dezhen Shen*

Cite This: *ACS Appl. Nano Mater.* 2022, 5, 17461−17467 Read Online

ACCESS | Metrics & More | Article Recommendations | Supporting Information

ABSTRACT: Emergent interfacial ferroelectricity has been surprisingly found in spatial inversion symmetry broken moiré systems, such as rhombohedral-stacked bilayer transition metal dichalcogenides (TMDs). However, the lattice dynamics of nanoscale polarization switching and ferroelectric hysteresis remain unclear. Here we report on the observation of phonon splitting of soliton networks in bilayer MoS_2 nanostructures with reconstructed moiré superlattices. By tuning a perpendicular displacement field, the interval of phonon splitting exhibits a distinct hysteresis behavior, which arises from solitons disentangling and lattice viscosity. Moreover, we demonstrate a proof-of-principle moiré ferroelectric tunneling junction. Our work presents a potential pathway for future moiré-based nanodevices.

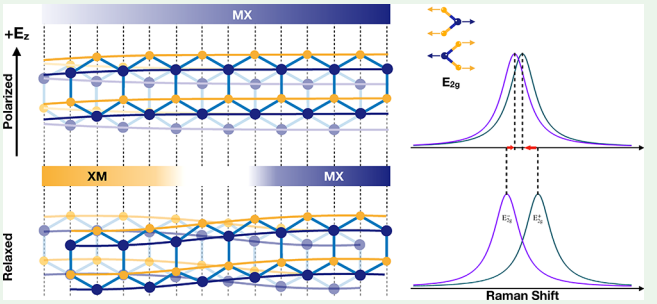

KEYWORDS: *moiré superlattice, reconstruction, nanoscale, ferroelectric, soliton, phonon splitting, tunneling*

INTRODUCTION

Moiré superlattices, arising from a mismatch in lattice constant or orientation between stacked monolayers, have emerged as powerful platforms for uncovering intriguing quantum states of matter, such as superconductivity,[1,2] correlated insulator,[3,4] orbital magnetism,[5] etc. With these inspiring advances, one of the primary concerns of moiré physics is exploring emergent phenomena which are absent from the individual constituents. For example, the long-period superlattices can fold the energy band into the moiré mini-Brillouin zone,[6] giving rise to a flat band and moiré potential,[7,8] and altering electronic correlations and topology, which is unattainable in the pristine band. In addition, engineering the symmetry breaking in moiré systems also offers multifaceted approaches to tuning the internal quantum degrees of freedom.[9,10] Recently, unconventional interfacial ferroelectricity has been found in lattice inversion symmetry broken homobilayer nanostructures, such as parallel-stacked bilayer hexagonal boron nitride (hBN),[11,12] and rhombohedral-stacked (R-stacked) bilayer transition metal dichalcogenides (TMDs).[13,14] The out-of-plane electric dipole moment stems from the local atomic registry and interlayer hybridization, switchable by in-plane interface sliding.[15,16] This kind of emergent ferroelectricity incorporated in atomically thin semiconducting R-stacked bilayer TMDs, namely, bilayer MoS_2, WS_2, $MoSe_2$, and WSe_2, shows a potential for the development of nonvolatile memory devices.[17,18] Moreover, combined with unique exciton properties (spin-valley locking, gate-tunable nontrivial topological phase transition) and interface polarization in R-stacked bilayer TMDs, this kind of nanoscale superlattice will inspire interest in future intelligent optoelectronic device applications.[19]

In marginally twisted R-stacked TMDs homobilayers, real moiré superlattices undergo lattice relaxation as a result of competition between intralayer strains and interlayer van der Waals (vdWs) coupling, leading to the reconstruction of energetically preferential domains with staggered stacking order.[20,21] This reconstruction is different from rigidly twisted lattices (Figure 1a,b). Commensurate domains possess alternating polarization, separated by a network of strain twist faults, termed moiré solitons,[22] acting as domain walls (DWs) (Figure 1c). The contrary evolution of adjacent domains under an out-of-plane electric displacement field has been proposed by theoretical studies[16] and has been shown by microscopy experiments.[13,14] Although some hysteretic behaviors of net polarization have been discovered, a microscopic sight of DW dynamics at the lattice level, which is fundamental for the ferroelectric response, remains inconclusive. Moreover, studies about resistive switching induced by moiré ferroelectricity are also insufficient.

Herein we reveal a notable correlation between the strain of moiré solitons and polarization hysteresis. At the soliton

Received: July 18, 2022
Accepted: September 8, 2022
Published: September 12, 2022

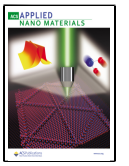

https://doi.org/10.1021/acsanm.2c03150
ACS Appl. Nano Mater. 2022, 5, 17461−17467

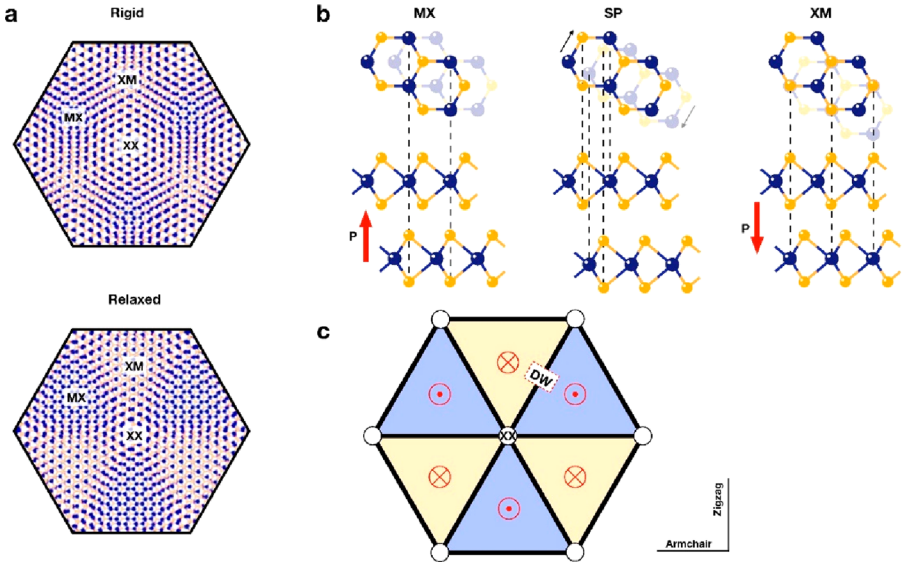

Figure 1. Schematic illustration of lattice reconstruction and the existence of polarization in a moiré superlattice. (a) Moiré superlattices present different lattice structures in a rigid and relaxed situation. (b) The origin of polarization in R-stacked bilayer MoS_2 (the yellow and blue balls are the sulfur atom and molybdenum atom, respectively). (c) Polarization direction and domain wall in reconstructed moiré superlattices.

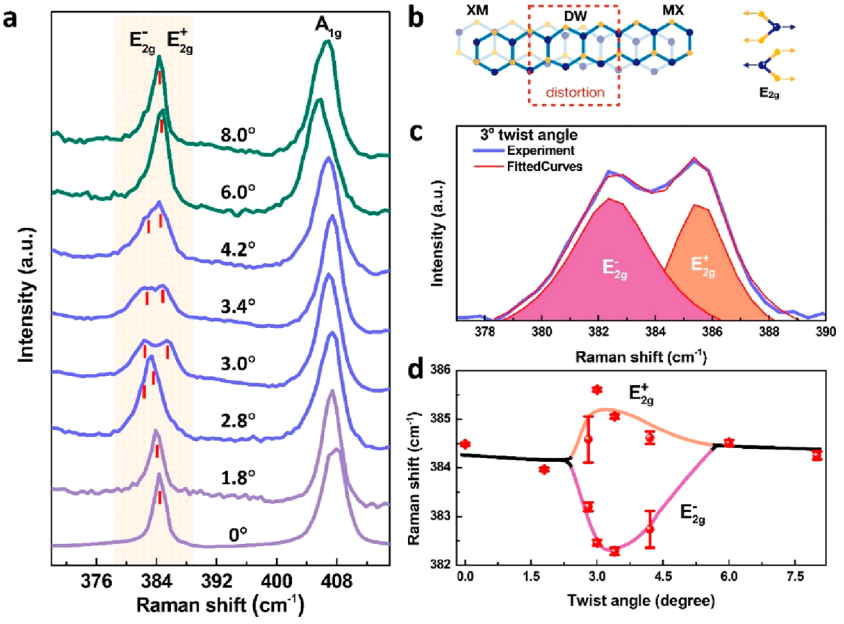

Figure 2. Raman spectra of R-stacked bi-MoS_2 and analysis. (a) Measured Raman spectra of bilayer MoS_2 for different twist angles. (b) The model of domain wall and intralayer phonon mode (the yellow and blue balls are the sulfur atom and molybdenum atoms, respectively), and the E_{2g} mode related to in-plane motion between molybdenum and sulfur atoms. (c) The blue line is the Raman spectrum of E_{2g} mode at the 3° twist angle, and the red line is the fitted curve. (d) Specific signatures of E_{2g} phonon splitting at different twist angles.

networks, local strain distorts the lattice and breaks the 3-fold rotational symmetry (C_3), causing the corresponding Raman vibrational mode (E_{2g}) splits. The out-of-plane electric field-dependent Raman frequency spacing allows us to identify DW motion, namely, the process of moiré solitons disentangling and entangling. Hence, we interpret the micromechanism of moiré ferroelectric hysteresis by using the interlayer lattice viscosity observed during moiré soliton disentanglement. Additionally, we demonstrate proof-of-principle moiré ferroelectric tunneling junctions to better elucidate the real function of net polar domains for the prospective applications of nonvolatile switching. Based on these new findings, moiré superlattices with inherent ferroelectricity offered a deeper insight into the strong correlation and topological physics recently observed in twisted bilayer TMDs. We also put forward promising scenarios for the novel electronic and optoelectronic devices with memory functions.

RESULTS AND DISCUSSION

In the range of small twisting angles of homobilayers, during the balance between intralayer and interlayer energies, the rigid atomic lattice suffers strain, along with moiré superlattice reconstructions. Quasi-one-dimensional moiré solitons, formed between polar domains, possess the information on the interlayer twist angle, which induces nonuniform uniaxial

https://doi.org/10.1021/acsanm.2c03150
ACS Appl. Nano Mater. 2022, 5, 17461−17467

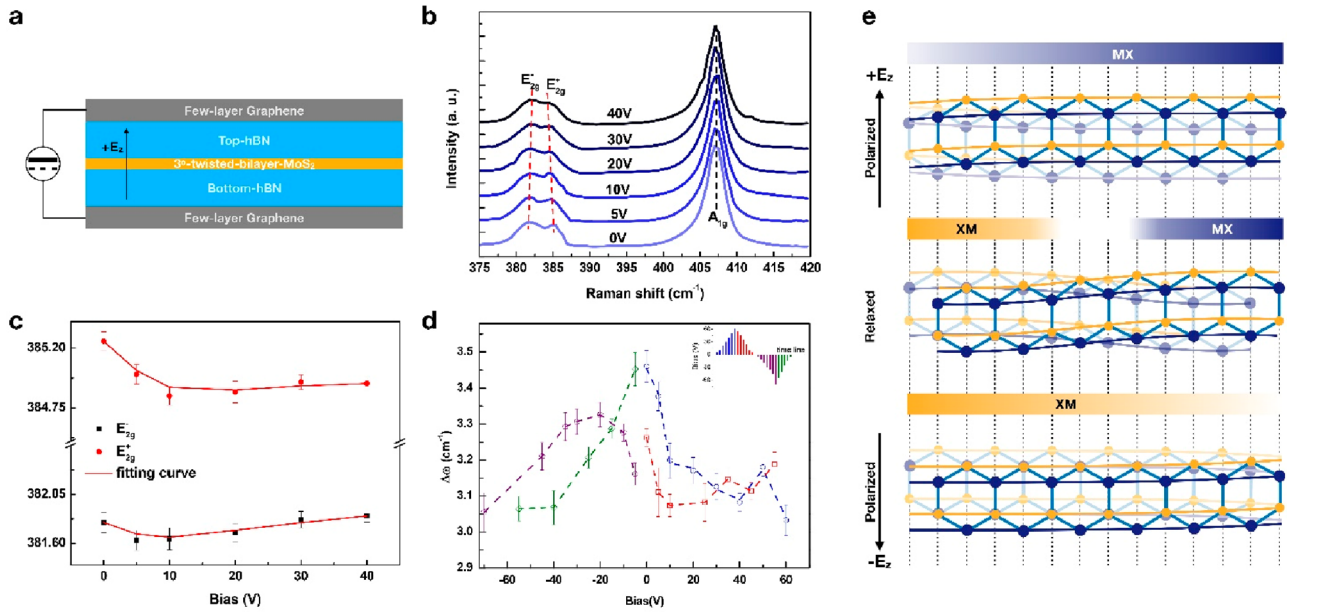

Figure 3. The electric field-dependent Raman spectroscopy, soliton disentangling, and lattice viscosity. (a) Schematic illustration of a bilayer twisted MoS_2 device. (b) Raman spectra under different out-of-plane electric fields in the wavenumber range of E_{2g} and A_{1g} modes. The excitation laser is 532 nm. (c) The fitting peaks of E_{2g}^- and E_{2g}^+ vs bias voltages. (d) The hysteresis curve of Raman frequency spacing of E_{2g} suggests the lattice viscosity effect. The applied voltages are shown in the inset (right-top). (d) Schematic illustration of moiré soliton disentangling under the out-of-plane electric field.

strain. The value of local strain on solitons is dependent on the twisting angle and degree of moiré superlattice reconstruction. In order to precisely control the twisting angle, we utilized the hBN-assisted tear-and-stack method[23] to make a set of MoS_2 bilayers, with twisting angles from 0° to 8°, which means realizing the R-stacked structure, and breaking global inversion symmetry and the out-of-plane mirror symmetry, concurrently (more details about the sample preparation can be found in Supporting Information). We performed Raman spectroscopy measurements that allow the identification of vibrational phonon modes in the reconstructed moiré superlattice, modified by the strain that originates from interlayer lattice relaxation. The angle evolution behavior of the Raman phonon peak positions of the twisted samples we studied is illustrated in Figure 2a, with data measured in the high-frequency range, and exhibited two typical intralayer vibration modes, known as E_{2g} and A_{1g}. Notably, the originally energy degenerate E_{2g} phonon vibrational mode is split into two peaks within a specific twisting angle range. Considering that the E_{2g} mode is caused by the opposing movements of two sulfur (S) atoms with respect to the molybdenum (Mo) atom in the in-plane direction (sketched in Figure 2b, right), phonon splitting indicates that C_3 symmetry has been broken by uniaxial strain. A slight shift of the A_{1g} mode with the twisting angle varying may be a result of the three-dimensional reconstruction of superlattices,[24] in which the out-of-plane relative motions of the S atoms can be modified. It also can be seen that the splitting of the E_{2g} mode is divided into three classes within the twisting angle range we studied, viz. from unimodality to bimodality, and reverted to the initial state finally, which signifies the degree of moiré superlattice reconstruction.[25]

As illustrated in Figure 2b, left, between two mirror-symmetrical commensurate domains, the moiré soliton, arising from interlayer lattice entanglement, endures significantly uniaxial strain alone in the armchair direction, due to the lattice relaxing. Twisting and reconstruction induced lattice distortions make part of the Mo−S bond stiffen and part soften, leading to E_{2g}^+ and E_{2g}^- shifting blue and red, respectively, relative to the initial E_{2g}, as shown in Figure 2c. Therefore, the spacing between E_{2g}^+ and E_{2g}^- reflects the degree of distortion of the soliton lattice. Likewise, strain reduction is also manifested in a reduction in spacing, see further discussion below.

Figure 2d shows more specific signatures of E_{2g} phonon splitting at different twist angles, from 0° to 8°, extracted from Figure 2a. The largest splitting is up to 3.4 cm^{-1} around 3.4°, which suggests the greatest strain. At the small twist angle ($0° < \theta < 2.8°$), although the moiré superlattice experienced a reconstruction, a minor twist fault in the soliton makes the lattice distortion insufficient, which is not enough to split the E_{2g} mode. Correspondingly, at the larger twist angle ($6° < \theta < 8°$), when the interlayer vdWs energy is not enough to offset the strain energy in the intralayer, the lattice relationship of the bilayer returns to a rigid state of monolayers; that is, the area of incommensurate atomic registries is increased instead, and the lattice distortion is not obvious. Remarkably, at the range of $2.8° < \theta < 6°$, the E_{2g} phonon mode splits into two distinct peaks, indicating that moiré solitons possess high strain locally. Because of the combination of twisting and relaxing, there are distorted lattices and a broken C_3 symmetry.

Since adjacent commensurate domains keep opposite dipole moments, an external electric field with an out-of-plane direction will drive an increase in the area of domains aligned with its own polarization.[13] The evolution of the domain area also implies the movement of the DW, that is, the movement of lattice solitons in the reconstructed moiré superlattice. Considering that the soliton movement will inevitably cause the change of strain, we employed electric field-dependent Raman spectroscopy to study the strain variation of soliton, where a dual-gate structure (Figure 3a) was fabricated to control the perpendicular displacement field. Notably, the twisting angle of R-stacked bilayer MoS_2, in this case, was fixed at 3°, for a higher strain, as we observed above, which is

https://doi.org/10.1021/acsanm.2c03150
ACS Appl. Nano Mater. 2022, 5, 17461−17467

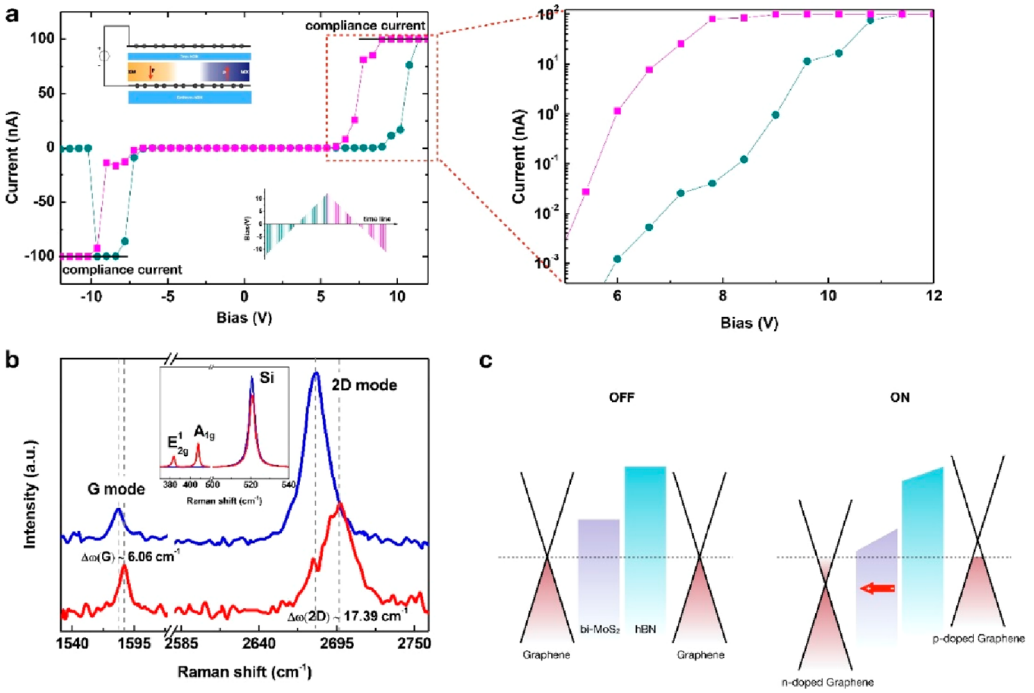

Figure 4. The moiré ferroelectric tunnel junction based on R-stacked bilayer MoS_2. (a) Current−voltage curves of the moiré ferroelectric device. Insert schematic illustration shows the structure of the device (left-top). Bilayer MoS_2 side is grounded. The applied bias voltages are shown in the inset (right-bottom). (b) The Raman spectra of graphene with/without the R-stacked bilayer MoS_2. The excitation laser is 532 nm. (c) Energy band schematic illustration for the OFF and ON states of our ferroelectric device.

expected to have more pronounced Raman peaks shifting varying with the electrical field.

Figure 3b shows the tendency of the high-frequency phonon mode (E_{2g} and A_{1g}) as a function of the external electric field. With the gate voltage increasing, the peak interval of E_{2g}^{+} and E_{2g}^{-} gradually diminishes (Figure 3b, c), while the peak of A_{1g} is stationary, indicating that the out-of-plane electric field affects the distorted lattices of solitons and tends to restore it to C_3 symmetry. Interestingly, as shown in Figure 3c, the E_{2g}^{+} manifests an apparent red-shift compared to E_2^{-}, which suggests the stiffness of the Mo−S bond of the solitons becoming softened. The red-shift of the peak position of E_{2g}^{+} tends to plateau after 20 V, which indicates that moiré soliton lattice strain driven by the perpendicular electric field reaches a new equilibrium. These electric field-dependent changes in the Raman phonon vibrational modes illustrate the dynamic evolution of the solitons' lattice, which can be phenomenologically illustrated in Figure 3e. When no gate voltage is applied, the soliton lattice is entangled and hosts a large lattice distortion along the armchair direction (middle of Figure 3e), so that the stacking order of the bilayer favorably transitions from MX (top metal atoms, bottom chalcogen atoms) to XM (top chalcogen atoms, bottom metal atoms). With the positive electric field applied, as shown at the top of Figure 3e, the MX domain aligned with the polarization direction of the external electric field will gradually dominate, and the corresponding moiré soliton will squeeze the space of the XM. Notably, the MX domain and XM domain always exist in Figure 3e, with the electric field just tuning the motion of the moiré soliton, which was reported in a previous study.[13] The movement of the moiré soliton appears as a disentangling process of the strained lattice, which is therefore accompanied by a tendency to restore C_3 symmetry. When applying the negative field, the moiré soliton cannot return to the initial state immediately as a result of the effect of lattice viscosity. With an increase in the negative field, the XM domain will gradually dominate, squeezing the space of MX. The bottom of Figure 3e illustrates the opposite situation.

To further characterize the hysteretic behavior of the movement of the moiré soliton, by applying a closed-loop voltage (inset of Figure 3d), the E_{2g} Raman frequency spacing vs voltage ($\Delta\omega-V$) measurement was performed in this dual-gate structure. The $\Delta\omega$ in Figure 3d shows a butterfly shaped hysteretic loop, indicating the ferroelectricity that was present. The attenuation of $\Delta\omega$ with the applied electric field marks the disentangling process of the soliton; however, the existence of the coercive field means that the interlayer lattice viscosity of the soliton plays a role in the re-entangling process. Therefore, solitons disentangling and lattice viscosity result in the switching of moiré ferroelectricity, as illustrated in Figure 3e.

The working mechanism of moiré ferroelectricity is fundamentally different from a conventional ferroelectric. As we discussed above, moiré ferroelectricity hosts two opposite polar domains in a reconstructed moiré unit cell. Thus, the overall interfacial barrier modulation induced by interlayer polarization in moiré superlattices will exhibit unique resistance-switching properties. Here, we fabricated a graphene/0°-R-stacked bi-MoS_2/hBN/graphene structure, a two-terminal vertical moiré ferroelectric tunnel junction (MFTJ), as shown in the upper left inset of Figure 4a. A current−voltage ($I-V$) measurement has been performed, where the bias voltage is in pulse mode (pulse duration, 200 ms) for reducing thermal effects, as shown in the lower right inset of Figure 4a. The corresponding tunneling current of the MFTJ presents a typical ON/OFF and hysteresis features above ~±5 V bias, suggesting the change of net moiré ferroelectric polarization. Remarkably, at a smaller bias voltage range, approximately from −5 V to +5 V, MFTJ exhibits a high resistance state. A

https://doi.org/10.1021/acsanm.2c03150
ACS Appl. Nano Mater. 2022, 5, 17461−17467

reasonable explanation is that an inadequate perpendicular electric field could not make enough of an area difference for the opposite polar domains (between MX and XM), generating an insufficient interface barrier modification for current tunneling. As the bias voltage increases, one of the polar domains gradually becomes dominant, which in turn puts the device in a low resistance state. Subsequently, when the applied voltage is reduced, the existence of interlayer lattice viscosity tends to maintain the lattice status and produce moiré ferroelectric hysteresis. The asymmetric curves in the positive and negative bias range of the MFTJ may be attributed to the global strain and the asymmetry of the domains caused by the nonuniform twisted angle. $I-V$ curves from the positive bias range can be seen in the right inset of Figure 4a; the switch ratio of the MFTJ is up to $\sim 10^4$ at room temperature. It should be noted that here the compliance current was set at 100 nA to prevent device breakdown. Thus, the device switch ratio above should be underestimated. Furthermore, for comparison purposes, we also fabricated the H-stacking bilayer MoS_2 tunneling junctions, which have no ferroelectric hysteresis behavior (Supporting Information Figure S6). Therefore, this confirms that the resistive state switching in the device originates from the switching in the moiré ferroelectric polarization.

For further study of the modified interface potential barrier, the Fermi level shift in graphene was confirmed by employing Raman spectroscopy measurements. As shown in Figure 4b, the G and 2D modes of the graphene in contact with R-stacked bilayer MoS_2 both have evident blue-shifts compared to the isolated graphene region. The main reason for these blue-shifts is the fact that the polarization field of the commensurate domains changes the doping level of the graphene. The Raman shift of the G-mode peak ($\Delta\omega$) is about 6.06 cm^{-1}, which can be used to quantitate the shift of the graphene Fermi level (ΔE_f), $|\Delta E_f| \approx \frac{\Delta\omega}{21} \approx 0.29$ eV.[26] During blue-shifting, the intensity ratio between the 2D and G modes (I_{2D}/I_G) decreased, which is the result of the doping effect by the polarization electric field.[27,28] Considering that the reconstructed R-stacked bilayer MoS_2 has two opposite polar domains, as mentioned above, graphene can be doped as electron- and hole-type alternatively. Therefore, a large proportion of graphene will be depleted, resulting in an underestimate of Fermi level shifts estimated by G-mode Raman shifts. This is also in consonance with the high resistance state of the $I-V$ curve in the small bias voltage range, where there is not enough net polar domain to change the interface potential barrier, further verifying the moiré ferroelectricity feature.

The band diagrams and operational principle of our MFTJ are shown in Figure 4c. The tunnel barrier is composed of bi-MoS_2 and hBN, with enough height/width, to allow nearly no thermionic emission and tunneling current at low bias voltage, namely, the OFF state. As the positive bias voltage increases, the perpendicular displacement field makes the polar domain (commensurate XM region) become dominant, associated with a net polarization field which emerged, whose effect is to shift the Fermi level of graphene from the Dirac point to n-type (the right side of Figure 4c). The extra shifting of the Fermi level in graphene decreases the average barrier height and width, inducing a larger tunneling current. Under reverse bias, a relatively symmetrical situation occurs (no schematic here).

CONCLUSION

We demonstrated the moiré soliton dynamics signatures and ferroelectric hysteresis in bilayer MoS_2 nanostructures with reconstructed moiré superlattices. The intrinsic lattice distortion in soliton networks is derived through the E_{2g} mode splitting in Raman spectroscopy. The shrinking of the phonon splitting under the penetration electric field suggests that the strain-broken C_3 symmetry tends to recover, indicating the occurrence of a moiré solitons disentanglement process. Then, the lattice viscosity has been verified by the coercive field that exists in the hysteresis of E_{2g} Raman frequency spacing. The MFTJ based on the graphene/0°-R-stacked bi-MoS_2/hBN/graphene vdWs nanostructure exhibits a high ratio of tunneling current, nearly 10^4. Unlike conventional ferroelectric switching, our device relies on the competition between polarized domains (XM/MX) to switch the net polarized electric field. Looking ahead, our findings point to many intriguing possibilities. For instance, the evolution of the soliton network and polarized domains may induce the topological phase transition of the energy band, thereby affecting the quantum geometry of the Bloch wave function, which is vitally manipulating the ground/excited state behavior of quasiparticles.[19,29] Moreover, moiré ferroelectricity also provides a new approach for in-memory computing (beyond von Neumann architecture).[30]

ASSOCIATED CONTENT

Supporting Information

The Supporting Information is available free of charge at https://pubs.acs.org/doi/10.1021/acsanm.2c03150.

Additional experimental details, materials, and methods, including details of the device fabrication procedure (PDF)

Video of the hBN-assisted tear-and-stack method (MP4)

AUTHOR INFORMATION

Corresponding Authors

Xiuhua Xie − *State Key Laboratory of Luminescence and Applications, Changchun Institute of Optics, Fine Mechanics and Physics, Chinese Academy of Sciences, Changchun 130033, China*; Email: xiexh@ciomp.ac.cn

Dezhen Shen − *State Key Laboratory of Luminescence and Applications, Changchun Institute of Optics, Fine Mechanics and Physics, Chinese Academy of Sciences, Changchun 130033, China*; Email: shendz@ciomp.ac.cn

Authors

Yanshuang Li − *State Key Laboratory of Luminescence and Applications, Changchun Institute of Optics, Fine Mechanics and Physics, Chinese Academy of Sciences, Changchun 130033, China; University of Chinese Academy of Sciences, Beijing 100049, China*

Huan Zeng − *State Key Laboratory of Luminescence and Applications, Changchun Institute of Optics, Fine Mechanics and Physics, Chinese Academy of Sciences, Changchun 130033, China; University of Chinese Academy of Sciences, Beijing 100049, China*; orcid.org/0000-0001-9782-322X

Binghui Li − *State Key Laboratory of Luminescence and Applications, Changchun Institute of Optics, Fine Mechanics and Physics, Chinese Academy of Sciences, Changchun 130033, China*

https://doi.org/10.1021/acsanm.2c03150
ACS Appl. Nano Mater. 2022, 5, 17461−17467

Jishan Liu − *Center for Excellence in Superconducting Electronics, State Key Laboratory of Functional Materials for Informatics, Shanghai Institute of Microsystem and Information Technology, Chinese Academy of Sciences, Shanghai 200050, China*

Shuangpeng Wang − *MOE Joint Key Laboratory, Institute of Applied Physics and Materials Engineering and Department of Physics and Chemistry, Faculty of Science and Technology, University of Macau, Macao, SAR 999078, P. R. China;* orcid.org/0000-0001-8464-4994

Dengyang Guo − *Department of Physics, Cavendish Laboratory, University of Cambridge, Cambridge CB3 0HE, United Kingdom*

Yuanzheng Li − *Key Laboratory of UV-Emitting Materials and Technology, Ministry of Education, Northeast Normal University, Changchun 130024, China;* orcid.org/0000-0002-4309-0160

Weizhen Liu − *Key Laboratory of UV-Emitting Materials and Technology, Ministry of Education, Northeast Normal University, Changchun 130024, China*

Complete contact information is available at: https://pubs.acs.org/10.1021/acsanm.2c03150

Author Contributions

[▽]Yanshuang Li and Huan Zeng contributed equally to this work.

Notes

The authors declare no competing financial interest.

All data that support the findings of this study within this paper and the Supporting Information are available from the corresponding authors upon reasonable request.

■ ACKNOWLEDGMENTS

We gratefully acknowledge X. Z. Yan and Z. Yu for their assistance with Raman measurements and fruitful discussions. This research is mainly supported by the National Natural Science Foundation of China (Grant Nos. 11727902). S.P. and X.H. gratefully acknowledge support from Multi-Year Research Grants (MYRG2020-00207-IAPME) from Research & Development Office at University of Macau. W.Z. and Y.Z. acknowledge support from Program of National Natural Science Foundation of China (Grant Nos.12004069 and 12074060).

■ REFERENCES

(1) Cao, Y.; Fatemi, V.; Fang, S.; Watanabe, K.; Taniguchi, T.; Kaxiras, E.; Jarillo-Herrero, P. Unconventional superconductivity in magic-angle graphene superlattices. *Nature* **2018**, *556* (7699), 43−50.

(2) Park, J. M.; Cao, Y.; Watanabe, K.; Taniguchi, T.; Jarillo-Herrero, P. Tunable strongly coupled superconductivity in magic-angle twisted trilayer graphene. *Nature* **2021**, *590* (7845), 249.

(3) Xu, Y.; Liu, S.; Rhodes, D. A.; Watanabe, K.; Taniguchi, T.; Hone, J.; Elser, V.; Mak, K. F.; Shan, J. Correlated insulating states at fractional fillings of moiré superlattices. *Nature* **2020**, *587* (7833), 214−218.

(4) Huang, X.; Wang, T.; Miao, S.; Wang, C.; Li, Z.; Lian, Z.; Taniguchi, T.; Watanabe, K.; Okamoto, S.; Xiao, D.; Shi, S.; Cui, Y. Correlated insulating states at fractional fillings of the WS_2/WSe_2 moiré lattice. *Nat. Phys.* **2021**, *17* (6), 715−719.

(5) Liu, J.; Dai, X. Orbital magnetic states in moire graphene systems. *Nature Reviews Physics* **2021**, *3* (5), 367−382.

(6) Torma, P.; Peotta, S.; Bernevig, B. A. Superconductivity, superfluidity and quantum geometry in twisted multilayer systems. *Nature Reviews Physics* **2022**, *4*, 528.

(7) Zhang, Z.; Wang, Y.; Watanabe, K.; Taniguchi, T.; Ueno, K.; Tutuc, E.; LeRoy, B. J. Flat bands in twisted bilayer transition metal dichalcogenides. *Nat. Phys.* **2020**, *16* (11), 1093−1096.

(8) Shabani, S.; Halbertal, D.; Wu, W.; Chen, M.; Liu, S.; Hone, J.; Yao, W.; Basov, D. N.; Zhu, X.; Pasupathy, A. N. Deep moiré potentials in twisted transition metal dichalcogenide bilayers. *Nat. Phys.* **2021**, *17* (6), 720−725.

(9) Kennes, D. M.; Claassen, M.; Xian, L.; Georges, A.; Millis, A. J.; Hone, J.; Dean, C. R.; Basov, D. N.; Pasupathy, A. N.; Rubio, A. Moiré heterostructures as a condensed-matter quantum simulator. *Nat. Phys.* **2021**, *17* (2), 155−163.

(10) Du, L.; Hasan, T.; Castellanos-Gomez, A.; Liu, G.-B.; Yao, Y.; Lau, C. N.; Sun, Z. Engineering symmetry breaking in 2D layered materials. *Nature Reviews Physics* **2021**, *3* (3), 193−206.

(11) Yasuda, K.; Wang, X.; Watanabe, K.; Taniguchi, T.; Jarillo-Herrero, P. Stacking-engineered ferroelectricity in bilayer boron nitride. *Science* **2021**, *372* (6549), 1458−1462.

(12) Vizner Stern, M.; Waschitz, Y.; Cao, W.; Nevo, I.; Watanabe, K.; Taniguchi, T.; Sela, E.; Urbakh, M.; Hod, O.; Ben Shalom, M. Interfacial ferroelectricity by van der Waals sliding. *Science* **2021**, *372* (6549), 1462−1466.

(13) Weston, A.; Castanon, E. G.; Enaldiev, V.; Ferreira, F.; Bhattacharjee, S.; Xu, S.; Corte-Leon, H.; Wu, Z.; Clark, N.; Summerfield, A.; Hashimoto, T.; Gao, Y.; Wang, W.; Hamer, M.; Read, H.; Fumagalli, L.; Kretinin, A.; Haigh, S.; Kazakova, O.; Geim, K.; Fal'ko, V.; Gorbachev, R. Interfacial ferroelectricity in marginally twisted 2D semiconductors. *Nat. Nanotechnol.* **2022**, *17* (4), 390−395.

(14) Wang, X.; Yasuda, K.; Zhang, Y.; Liu, S.; Watanabe, K.; Taniguchi, T.; Hone, J.; Fu, L.; Jarillo-Herrero, P. Interfacial ferroelectricity in rhombohedral-stacked bilayer transition metal dichalcogenides. *Nat. Nanotechnol.* **2022**, *17* (4), 367−371.

(15) Bennett, D.; Remez, B. On electrically tunable stacking domains and ferroelectricity in moiré superlattices. *Npj 2d Materials and Applications* **2022**, *6* (1), 7 DOI: 10.1038/s41699-021-00281-6.

(16) Bennett, D. *Theory of Polar Domains in Moiré Heterostructures* **2022**. Preprint at DOI: 10.48550/arXiv.2203.01979(2022).

(17) Rogee, L.; Wang, L.; Zhang, Y.; Cai, S.; Wang, P.; Chhowalla, M.; Ji, W.; Lau, S. P. Ferroelectricity in untwisted heterobilayers of transition metal dichalcogenides. *Science (New York, N.Y.)* **2022**, *376* (6596), 973−978.

(18) Wu, M. Two-Dimensional van der Waals Ferroelectrics: Scientific and Technological Opportunities. *ACS Nano* **2021**, *15* (6), 9229−9237.

(19) Ma, C.; Yuan, S.; Cheung, P.; Watanabe, K.; Taniguchi, T.; Zhang, F.; Xia, F. Intelligent infrared sensing enabled by tunable moiré quantum geometry. *Nature* **2022**, *604* (7905), 266−272.

(20) Carr, S.; Massatt, D.; Torrisi, S. B.; Cazeaux, P.; Luskin, M.; Kaxiras, E. Relaxation and domain formation in incommensurate two-dimensional heterostructures. *Phys. Rev. B* **2018**, *98* (22), 224102 DOI: 10.1103/PhysRevB.98.224102.

(21) Weston, A.; Zou, Y.; Enaldiev, V.; Summerfield, A.; Clark, N.; Zolyomi, V.; Graham, A.; Yelgel, C.; Magorrian, S.; Zhou, M.; Zultak, J.; Hopkinson, D.; Barinov, A.; Bointon, T.; Kretinin, A.; Wilson, N.; Beton, P.; Fal'ko, V.; Haigh, S.; Gorbachev, R. Atomic reconstruction in twisted bilayers of transition metal dichalcogenides. *Nat. Nanotechnol.* **2020**, *15* (7), 592−597.

(22) Turkel, S.; Swann, J.; Zhu, Z.; Christos, M.; Watanabe, K.; Taniguchi, T.; Sachdev, S.; Scheurer, M. S.; Kaxiras, E.; Dean, C. R.; Pasupathy, A. N. Orderly disorder in magic-angle twisted trilayer graphene. *Science* **2022**, *376* (6589), 193−199.

(23) Kim, K.; Yankowitz, M.; Fallahazad, B.; Kang, S.; Movva, H. C. P.; Huang, S.; Larentis, S.; Corbet, C. M.; Taniguchi, T.; Watanabe, K.; Banerjee, S. K.; LeRoy, B. J.; Tutuc, E. van der Waals Heterostructures with High Accuracy Rotational Alignment. *Nano Lett.* **2016**, *16* (3), 1989−1995.

(24) Li, H.; Li, S.; Naik, M. H.; Xie, J.; Li, X.; Wang, J.; Regan, E.; Wang, D.; Zhao, W.; Zhao, S.; Kahn, S.; Yumigeta, K.; Blei, M.; Taniguchi, T.; Watanabe, K.; Tongay, S.; Zettl, A.; Louie, S. G.;

Wang, F.; Crommie, M. F. Imaging moire flat bands in three-dimensional reconstructed WSe_2/WS_2 superlattices. *Nat. Mater.* **2021**, *20* (7), 945−950.
(25) Quan, J.; Linhart, L.; Lin, M.-L.; Lee, D.; Zhu, J.; Wang, C.-Y.; Hsu, W.-T.; Choi, J.; Embley, J.; Young, C.; Taniguchi, T.; Watanabe, K.; Shih, C. K.; Lai, K.; MacDonald, A. H.; Tan, P. H.; Libisch, F.; Li, X. Q. Phonon renormalization in reconstructed MoS_2 moiré superlattices. *Nat. Mater.* **2021**, *20* (8), 1100−1105.
(26) Chen, C.-F.; Park, C.-H.; Boudouris, B. W.; Horng, J.; Geng, B.; Girit, C.; Zettl, A.; Crommie, M. F.; Segalman, R. A.; Louie, S. G.; Wang, F. Controlling inelastic light scattering quantum pathways in graphene. *Nature* **2011**, *471* (7340), 617−620.
(27) Das, A.; Pisana, S.; Chakraborty, B.; Piscanec, S.; Saha, S. K.; Waghmare, U. V.; Novoselov, K. S.; Krishnamurthy, H. R.; Geim, A. K.; Ferrari, A. C.; Sood, A. K. Monitoring dopants by Raman scattering in an electrochemically top-gated graphene transistor. *Nat. Nanotechnol.* **2008**, *3* (4), 210−215.
(28) Wu, J.-B.; Lin, M.-L.; Cong, X.; Liu, H.-N.; Tan, P.-H. Raman spectroscopy of graphene-based materials and its applications in related devices. *Chem. Soc. Rev.* **2018**, *47* (5), 1822−1873.
(29) Sinha, S.; Adak, P. C.; Chakraborty, A.; Das, K.; Debnath, K.; Sangani, L. D. V.; Watanabe, K.; Taniguchi, T.; Waghmare, U. V.; Agarwal, A.; Deshmukh, M. M. Berry curvature dipole senses topological transition in a moiré superlattice. *Nat. Phys.* **2022**, *18*, 765.
(30) Liu, C.; Chen, H.; Wang, S.; Liu, Q.; Jiang, Y.-G.; Zhang, D. W.; Liu, M.; Zhou, P. Two-dimensional materials for next-generation computing technologies. *Nat. Nanotechnol.* **2020**, *15* (7), 545−557.

https://doi.org/10.1021/acsanm.2c03150
ACS Appl. Nano Mater. 2022, 5, 17461−17467